Combust. Theory Modelling **3** (1999) P177- 198 Printed in the UK PII: S1364-7830(99)92097-1

# An adaptive two-dimensional wavelet–vaguelette algorithm for the computation of flame balls

Henning Bockhorn†, Jochen Fröhlich‡‖ and Kai Schneider†§

† Institut für Chemische Technik, Universität Karlsruhe, Kaiserstraße 12, 76128 Karlsruhe, Germany
‡ Konrad-Zuse-Zentrum Berlin, Heilbronner Straße 10, 10711 Berlin, Germany
§ Centre de Physique Théorique, CNRS Luminy, Case 907, 13288 Marseille Cedex 09, France

Received 27 February 1998, in final form 4 August 1998

**Abstract.** This paper is concerned with the numerical simulation of two-dimensional flame balls. We describe a Galerkin-type discretization in an adaptive basis of orthogonal wavelets. The solution is represented by means of a reduced basis being adapted in each time step. This algorithm is applied to compute the evolution of circular and elliptic thermodiffusive flames. In particular, we study the influence of the Lewis number, the strength of radiative losses and of the initial radius. The results show different scenarios. We find repeated splitting of the flame ball which is studied in some detail, extinction after excessive growth and also obtain quasi-steady flame balls.

## 1. Introduction

The design of efficient, low-pollution combustion engines and the assessment of fire and explosion hazards in chemical plants, mine shafts, etc requires a profound knowledge of the behaviour of premixed gas flames near extinction or stability limits. Since under these conditions the flames are very sensitive—micro-gravity constitutes a suitable environment for the investigation of such phenomena. Due to the absence of buoyant convection, which on Earth generates convection, strongly influencing the reaction zone, other transport mechanisms, such as Lewis number effects or radiation can be investigated in detail. To elucidate these questions several micro-gravity ($\mu$g) experiments in drop towers, aircraft and even in the space shuttle have been carried out and are still planned for the future¶. Typically these experiments are performed in a combustion chamber containing a quiescent, premixed lean gas mixture with a reactant of small Lewis number. A point ignition leads to a flame that rapidly breaks up into cells, a phenomenon caused by cellular instability at small Lewis numbers. In some cases, however, steady spherical flame balls form which are not supported by any source of reactants or sink of products in their centre [32]. The conceptual importance of such a configuration resides in the possibility of investigating flammability limits. In general, these limits depend to a very large extent on the actual device which is used for an experiment. Flame balls exist far from any boundary. They are related to near-quenching conditions and can exist for a relatively long time. Hence, they might allow the determination of flammability limits which only depend on the reaction mechanism, not on a particular set-up, which would then in a certain way be ‘absolute’.

‖ Present address: Institut für Hydrodynamik, Universität Karlsruhe, Kaiserstraße 12, D-76128 Karlsruhe, Germany.
¶ Information about ongoing research at NASA is available at http://cpl.usc.edu/sofball/

1364-7830/99/000001+22$19.50  

Important experimental work on flame balls has been done by Ronney, who investigated stable flame balls in lean $H_2$–air mixtures in $\mu$g [32]. This was the starting point for further theoretical and experimental studies reviewed in [2, 33]. The theoretical analysis has mainly been carried out by asymptotic methods and matched expansions. Historically, Zeldovich [40] already considered flame balls without heat loss and proved the existence of a stationary solution for a certain radius of the flame, the so-called Zeldovich radius. However, it has later been shown that this solution is always unstable [7, 16]. With additional heat loss due to radiation, however, spherical flames can be stabilized. In [3, 4, 34] the stability with respect to one-dimensional perturbations, i.e. uniform growth or decrease of the radius, has been considered. In [5] the stability with respect to three-dimensional perturbations was investigated distinguishing also between far-field and near-field heat losses. A more sophisticated model for radiation based on a partial differential equation (PDE) for the heat loss has later been employed in [28] for a similar stability analysis.

Numerical simulations of flame balls are relatively rare. In [5] a one-dimensional equation governing the flame ball radius is solved numerically. Later, Buckmaster *et al* [6] simulated flame balls with imposed spherical symmetry (one-dimensional problem) using realistic $H_2$ kinetics and obtained good agreement with the experiments. In [39] numerical simulations of this configuration were also undertaken with complex chemistry. A relatively similar problem, the one of an inward burning spherical flame with radiation, has recently been investigated numerically in [25], also with imposed spherical symmetry. In [26] the influence of radiation on the formation of cellular structures has been studied for planar premixed flames by two-dimensional numerical simulation. This local extinction of premixed flames at low Lewis number was first observed by Denet and Haldenwang in [14] for the adiabatic case. In all the direct simulations cited above, the thermodiffusive model has been used '*in order to reduce the computations while apparently preserving the major aspects of the relevant phenomenology*' [26]. In the present paper we also employ this classical framework with a one-step irreversible exothermic reaction and Arrhenius kinetics.

A well known fact for the numerical simulation of combustion problems with full resolution of the flame front is that adaptive methods are highly recommended to cope with the different spatial length scales that have to be resolved, see e.g. [15]. Recently, multiscale methods (and wavelet methods fall into this category) have become of increasing interest in solving a large class of integral and differential equations. This is motivated by their efficient, i.e. sparse and/or well conditioned, representation of the involved operators and the solution itself. Essentially, the existing approaches rely on the simultaneous localization of wavelets and wavelet-like functions in space and frequency. Different algorithms have been devised which exploit this feature such as the method of Liandrat and Tchamitchian [27] or the collocation procedure in [9]. A detailed review of the literature on this subject is beyond the scope of this paper but has been undertaken in [12, 23] to which the reader is referred.

In the past, we have developed a one-dimensional adaptive wavelet discretization procedure in space for parabolic PDEs [20], which was used together with an additional Fourier discretization to compute cellular flames. Later the algorithm was substantially improved and extended for two dimensions [22]; this reference, however, contains very little information on the two-dimensional case so that part of the present text is concerned with filling this gap. The developed method is based on a Petrov–Galerkin scheme with the trial functions constituting a lacunary two-dimensional wavelet basis. The test functions are constructed in order to diagonalize the stiffness matrix resulting from a certain class of operators. In [21] the method has been extended to solve the Navier–Stokes equations for two-dimensional turbulence; see also [19] for a recent overview on wavelets in turbulence.

The aim of the present paper is the investigation of flame balls by the numerical simulation of the governing PDEs. After presenting the physical model in section 2 we describe the complete two-dimensional form of the adaptive wavelet algorithm (section 3). Different aspects such as the employed functions and the two-dimensional adaption strategy are illustrated. Section 4 reports original results on the simulation of flame balls. We start with the computation of an elliptic flame at unitary Lewis number which relaxes to a circular flame. Subsequently, the influence of radiation on the self-fragmentation of elliptical flames at low Lewis number is analysed. Interesting pattern formation is observed and its dependency on the radiative cooling is studied. We then address the question of stable flame structures in the considered setting. Indeed, quasi-steady flame balls could be obtained and constitute a substantial achievement of the present paper. The paper ends with a conclusive discussion of the employed method and the computed results as well as perspectives on future work.

## 2. Considered problem

In figure 1 a flame ball is represented schematically together with the physical mechanisms involved. For adiabatic conditions the flame would propagate outwards with its own deflagration speed. Heat losses due to radiation, however, slow down the propagation as they reduce the reaction rate and decrease the pre-heating ahead of the flame. For lean mixtures with low Lewis number this can yield a stationary or very slowly propagating flame which is then supplied with reactant only by diffusion of species towards the flame. If the propagation of the flame is slow the convection generated by the expansion of the gas remains small. Hence it is justified to neglect convection in the considered equations. A further approximation step is to assume the density and other thermodynamic properties of the gas to be constant. First, it should be observed that the actual temperature rise in the considered flames is indeed rather low compared to other practical flames. Second, note that for a steady flame in a quiescent atmosphere no gas is convected across the flame. This suppresses the Darrieus–Landau mechanism even for large density ratios across the flame. Hence, although the density is not constant all over the domain in the experiment this does not alter the mechanism of the thermodiffusive instability. The constant-density approximation is therefore a valid model for steady and slowly propagating flame balls. These so-called thermodiffusive equations have been used in a number of papers concerned with the theoretical stability analysis of

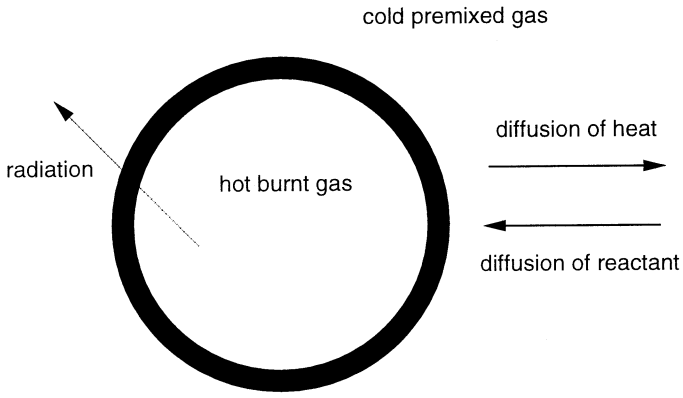


**Figure 1.** Schematic view of a flame ball and the involved mechanisms.

flame balls such as [4, 5, 28, 34]. We employ them here in dimensionless form with one-step kinetics [8]

$$\partial_t T - \nabla^2 T = \omega - s \tag{1}$$

$$\partial_t Y - \frac{1}{Le}\nabla^2 Y = -\omega \tag{2}$$

$$\omega = \frac{\beta^2}{2Le} Y \exp\left(\frac{\beta(T-1)}{1+\alpha(T-1)}\right). \tag{3}$$

Therein, $Le$ is the Lewis number, $T$ denotes the dimensionless reduced temperature $T = (\bar{T} - \bar{T}_u)/(\bar{T}_b - \bar{T}_u)$, and $Y$ the species concentration nondimensionalized with the concentration of the fresh mixture. The reference length is the (thermal) flame thickness and the reference velocity is the adiabatic propagation rate. The overbar designates dimensional quantities, the indices $u$ and $b$ refer to the unburnt and to the burnt state without heat loss, respectively. Hence, both variables $T$ and $Y$ range between zero and one with $Y = 1$, $T = 0$ for the unburnt and $Y = 0$, $T = 1$ for the (adiabatically) burnt limit. The Arrhenius term for the reaction rate $\omega$ incorporates the dimensionless activation energy $\beta$ (Zeldovich number) and the temperature ratio $\alpha = (\bar{T}_b - \bar{T}_u)/\bar{T}_b$. The heat loss due to radiation is modelled by a function $s = s(T)$ with

$$s = c\frac{\bar{T}^4 - \bar{T}_u^4}{(\bar{T}_b - \bar{T}_u)^4} \tag{4}$$

where $c$ depends on the Stefan Boltzmann constant and the Planck length. This is a relatively simple model which only accounts for the far-field losses in the optically thin limit. On the other hand, no further approximation by linearization is applied. Different approaches for the modelling of radiation can also be found in the literature, see e.g. [28]. However, up to now their impact on the resulting solution has not been totally clear. For the time being we therefore restrict ourselves to the expression in (4) as was also done in [26].

## 3. Adaptive wavelet algorithm

This section presents the essential features of the two-dimensional wavelet algorithm for parabolic PDEs in a concise way. Its mathematical properties have been investigated in [22], where accompanying numerical tests can be found as well. Concerning an introduction to the theory of wavelets we refer to textbooks such as [10, 13, 30]. In [22] the one-dimensional algorithm has been fully detailed and its mathematical properties have been investigated. The two-dimensional case could, however, only be sketched briefly, but the algorithm was tested with a two-dimensional Helmholtz-type equation and the initial phase of a laminar flame.

### *3.1. Time discretization of the evolution equations*

The thermodiffusive equations (1) and (2) can be written in the general form of a nonlinear evolution equation

$$\partial_t U + K(U) - F(U) = 0 \tag{5}$$

where $K$ denotes a linear differential operator in space and where the nonlinear function $F$ constitutes the only coupling between the components of the vector of unknowns $U$. This equation is discretized in time by a semi-implicit finite-difference scheme of second order,

$$(\gamma I + K)U^{n+1} = \tfrac{4}{3}\gamma U^n - \tfrac{1}{3}\gamma U^{n-1} + F(2U^n - U^{n-1}) \tag{6}$$

with time step $\Delta t$, $\gamma = 2/(3\Delta t)$, and $I$ representing the identity.

For the spatial discretization we use a Petrov–Galerkin scheme (method of weighted residuals). Each component of the solution $U$ is developed into a set of trial functions. The minimization of the weighted residual of (6) requires that the projection of the equation onto a space of test functions vanishes. The proposed algorithm is based on a particular choice of test and trial functions in terms of wavelets and their operator–orthogonal vaguelettes which will be described below.

Equation (6) can be solved component-wise for a given right-hand side. Hence, the method is presented here considering the scalar equation

$$Lu = f \tag{7}$$

with $L = \gamma I - C(\partial_{xx} + \partial_{yy})$. The constant $C$ includes length scaling and the diffusion coefficient (1 or $1/Le$, respectively). The operator $L$ has constant coefficients and is related to the symbol $\sigma(\xi_x, \xi_y) = \gamma I + 4\pi^2 C(\xi_x^2 + \xi_y^2)$. Observe that $\gamma > 0$ yields $\sigma > 0$ which is another way to say that $L$ is an elliptic operator with an inhomogeneous symbol.

### *3.2. Periodic two-dimensional wavelets*

Let us briefly recall the required notation. A periodic multiresolution (MRA) of $L^2(\mathbb{T})$ is a sequence of embedded subspaces $V_j \subset V_{j+1}$, $j \in \mathbb{N}_0$ of $L^2(\mathbb{T})$, where the latter denotes the space of real-valued square-integrable 1-periodic functions living on the torus $\mathbb{T} = \mathbb{R}/\mathbb{Z}$. This space is equipped with the inner product $\langle f, g\rangle = \int_{\mathbb{T}} f(x)\, g(x)\, \mathrm{d}x$ and the corresponding norm $\|f\|_2^2 = \langle f, f\rangle$. A refinable function $b^{\mathbb{R}}(x) \in L^2(\mathbb{R})$ generating an MRA of $L^2(\mathbb{R})$ through $b_{ji}^{\mathbb{R}}(x) = 2^{j/2} b^{\mathbb{R}}(2^j x - i)$ can be used to obtain a periodic MRA via [30, 31]

$$b_{ji}(x) = \sum_{n\in\mathbb{Z}} b_{ji}^{\mathbb{R}}(x+n) \qquad x \in \mathbb{T} \qquad \text{or} \qquad \hat{b}(k) = \hat{b}^{\mathbb{R}}(k) \qquad k \in \mathbb{Z} \tag{8}$$

with

$$\hat{b}(k) = \int_0^1 b(x)\, \mathrm{e}^{-2\pi \mathrm{i} k x}\, \mathrm{d}x \qquad \hat{b}^{\mathbb{R}}(\omega) = \int_{-\infty}^{\infty} b^{\mathbb{R}}(x)\, \mathrm{e}^{-2\pi \mathrm{i}\omega x}\, \mathrm{d}x. \tag{9}$$

These relations permit one to deduce scaling functions $\phi_{j,i}$, wavelets $\psi_{j,i}$ and the required filters from the non-periodic case. The cardinal Lagrange function in $V_j$ is given by

$$\widehat{S}_{ji}(k) = \frac{2^{-j}\hat{b}_{ji}(k)}{\sum_{n\in\mathbb{Z}} \hat{b}_{ji}(k + 2^j n)} \qquad k \in \mathbb{Z} \tag{10}$$

provided that the denominator is different from zero. By definition

$$S_{j,0}\left(\frac{i}{2^j}\right) = \delta_{i,0} \qquad V_j = \operatorname{span}\{S_{j,i}\}_{i=0,\ldots,2^j-1}. \tag{11}$$

The function $S$ allows an easy connection between sampled values in physical space and coefficients. This is relevant in order to evaluate nonlinear terms of PDEs in physical space. A collocation projection then is well suited for returning to the wavelet coefficient space. In the classical case the scaling functions $\phi_{jk}$ constitute an orthonormal basis of $V_j$, so that $\langle \phi_{j,i}, \phi_{j,k}\rangle = \delta_{i,k}$. The orthogonal complement space $W_j = V_{j+1} \ominus V_j$ is spanned by the orthonormal wavelets $\psi_{ji}(x) = \psi_{j0}(x - i/2^j)$, $i = 0, 2^j - 1$.

A two-dimensional MRA, i.e. an MRA of $L^2(\mathbb{T}^2)$ can be obtained through the tensor product of two one-dimensional MRAs of $L^2(\mathbb{T})$ defining $\boldsymbol{V}_j = V_j \otimes V_j$ [30]. The related bivariate orthogonal scaling functions are

$$\phi_{j,i_x,i_y}(x, y) = \phi_{j,i_x}(x)\, \phi_{j,i_y}(y). \tag{12}$$

Hence, the scale parameter $j$ simultaneously controls the dilation in $x$ and $y$. The orthogonal complement $\boldsymbol{W}_j = \boldsymbol{V}_j \ominus \boldsymbol{V}_{j+1}$ is then generated by three different wavelets

$$\psi^{\varepsilon}_{j,i_x,i_y}(x,y) = \begin{cases} \psi_{j,i_x}(x)\,\phi_{j,i_y}(y) & \varepsilon = 1 \\ \phi_{j,i_x}(x)\,\psi_{j,i_y}(y) & \varepsilon = 2 \\ \psi_{j,i_x}(x)\,\psi_{j,i_y}(y) & \varepsilon = 3 \end{cases} \tag{13}$$

for $j \geqslant 0$ and $i_x, i_y = 0, \ldots, 2^j - 1$.

This allows one to decompose $L^2(\mathbb{T}^2)$ into mutually orthogonal hierarchical subspaces

$$L^2(\mathbb{T}^2) = \boldsymbol{V}_0 \oplus_{j \geqslant 0} \boldsymbol{W}_j. \tag{14}$$

Correspondingly, any function $u \in L^2(\mathbb{T}^2)$ which is at least continuous† can be projected onto $\boldsymbol{V}_J$ by collocation

$$u_J(x,y) = \sum_{i_x=0}^{2^J-1} \sum_{i_y=0}^{2^J-1} u\left(\frac{i_x}{2^J}, \frac{i_y}{2^J}\right) S_{J,i_x,i_y}(x,y) \tag{15}$$

using the two-dimensional cardinal Lagrange function

$$S_{j,i_x,i_y}(x,y) = S_{j,i_x}(x)\,S_{j,i_y}(y). \tag{16}$$

It can then be expressed as

$$u_J(x,y) = c_{0,0,0}\,\phi_{0,0,0}(x,y) + \sum_{j=0}^{J-1} \sum_{i_x=0}^{2^j-1} \sum_{i_y=0}^{2^j-1} \sum_{\varepsilon=1}^{3} d^{\varepsilon}_{j,i_x,i_y}\,\psi^{\varepsilon}_{j,i_x,i_y}(x,y) \tag{17}$$

with coefficients

$$d^{\varepsilon}_{j,i_x,i_y} = \langle u, \psi^{\varepsilon}_{j,i_x,i_y} \rangle \qquad c_{0,0,0} = \int_{\mathbb{T}^2} u(x,y)\,\mathrm{d}x\,\mathrm{d}y \tag{18}$$

using the fact that $\phi_{0,0,0} = 1$.

Representing a function in terms of wavelet coefficients has the following advantages. Smooth functions yield rapid decay of the coefficients in scale (depending on the number of vanishing moments of $\psi_{ji}$). At locations where $u$ develops a singularity or an 'almost singularity' only local coefficients have to be retained (depending on the decay of $\psi_{ji}$ in space). Second, all employed basis functions are mutually orthogonal, a property which is the keystone of the algorithm below.

### *3.3. Adaptive discretization*

The approximation properties of wavelets furnish decay rates and estimations of the truncation error for given regularity of the function $u$ in (17). The asymptotic behaviour of linear and in particular nonlinear approximation using wavelets is treated in [17, 18, 30]. However, in practical computations the truncation error is estimated from the decay of the computed wavelet coefficients so that we need not go into details of the theory here. If the smoothness of $u$ varies strongly in space it is appropriate to use an adaptive discretization. For a wavelet discretization such as (17) this is accomplished by restricting the full index set

$$\Lambda_J = \{(j, i_x, i_y, \varepsilon) | j = 0, \ldots, J-1, i_x = 0, \ldots, 2^j - 1, i_x = 0, \ldots, 2^j - 1, \varepsilon = 1, 2, 3\} \tag{19}$$

† This is required to give a value of $f$ at a point a meaning, which is of course a prerequisite for collocation. To avoid technical details here we refer the reader to [1].

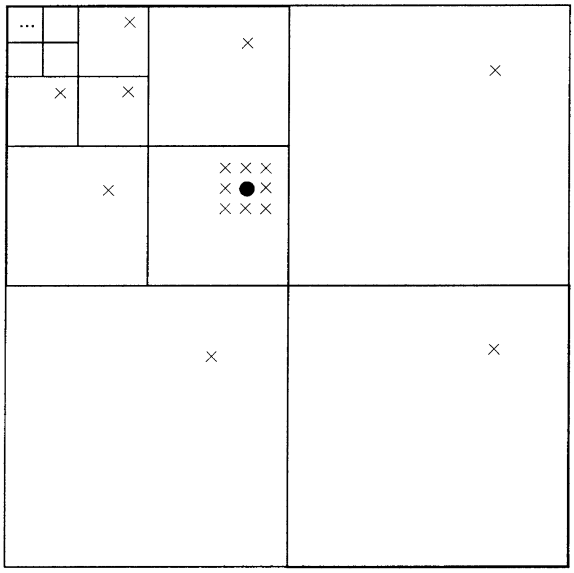

**Figure 2.** Scheme of the wavelet coefficients for a two-dimensional MRA and illustration of the applied neighbouring relation (see text).

to some subset $\Lambda_d \subset \Lambda_J$, depending on the required tolerance $\epsilon$. The elements designated by $\Lambda_d$ are termed the 'lacunary basis'. One is then interested in, roughly, retaining only coefficients with $|d^{\varepsilon}_{j,i_x,i_y}| > \epsilon$. Orthogonality of the basis and decay immediately relate this to the $L^2$ approximation error.

For an evolutionary problem discretized by a two-dimensional MRA this set can be estimated with a similar procedure as for a one-dimensional MRA used in [20, 27, 29]: from the previous time step the indices with coefficients larger than the tolerance $\epsilon$ are determined. These are then supplemented with the set of their neighbours in coefficient space. The easy definition of such a neighbouring set is an advantage of employing wavelets instead of wavelet packets [24]. The employed set is illustrated in figure 2. A coefficient $d^{\varepsilon}_{j,i_x,i_y}$ is placed at $x = 2^j(1 - \delta_{\varepsilon,1}) + i_x$, $y = 2^j(1 - \delta_{\varepsilon,2}) + i_y$ with the origin in the upper left-hand corner and the $y$-coordinate directed downwards. In each square $j$ and $\varepsilon$ are constant. We then define the nearest neighbours of the coefficient $d^3_{j,i_x,i_y}$ marked by a full dot as indicated by the crosses. The coefficients $d^1_{j,i_x,i_y}$ and $d^2_{j,i_x,i_y}$ have the same neighbours apart from the hull around them.

Of course, different definitions of a set of neighbours can be thought of. However, increasing this region generally results with the above adaption strategy in the computation of further coefficients smaller than $\epsilon$. Since their values are still used in the right-hand side of the equation solved in each time step this just amounts to computing with an effective tolerance smaller than the nominal one.

### *3.4. Operator-adapted two-dimensional vaguelettes*

In the present method the trial functions for $u$ are chosen to be the orthogonal periodic wavelets described in section 3.2. In order to determine the coefficients in (17) designated by $\Lambda_d$ a suitable weighted residuals projection has to be defined. Such a projection yields, in general, a matrix which has to be set up and inverted, i.e. a linear system has to be solved. For different

bases this matrix can have a special structure such as a block diagonal [11], e.g. applied in [38], or diagonal [27]. The latter strategy is used here when employing the functions $\theta$ defined below as test functions and avoids any linear system being assembled or solved. The particular advantage of using wavelets is that these, together with the resulting test functions, are well localized in space and frequency. This allows one to devise hierarchical decomposition algorithms through the application of appropriate filters as described in the following section.

For a sufficiently regular MRA the following functions can be defined:

$$\theta^{\varepsilon}_{j,i_x,i_y} = (L^*)^{-1}\psi^{\varepsilon}_{j,i_x,i_y} \qquad \mu^{\varepsilon}_{j,i_x,i_y} = L\psi^{\varepsilon}_{j,i_x,i_y} \tag{20}$$

$$\eta_{j,i_x,i_y} = (L^*)^{-1}\phi_{j,i_x,i_y} \qquad \nu_{j,i_x,i_y} = L\phi_{j,i_x,i_y}. \tag{21}$$

The superscript $*$ denotes the adjoint but may be omitted here because $L$ is self-adjoint ($\sigma$ is real). By construction these functions fulfil the bi-orthogonality relations

$$\langle\theta^{\varepsilon}_{j,i_x,i_y}, \mu^{\varepsilon'}_{k,m_x,m_y}\rangle = \delta_{jk}\delta_{i_x m_x}\delta_{i_y m_y}\delta_{\varepsilon\varepsilon'} \qquad \langle\eta_{j,i_x,i_y}, \nu_{j,k_x,k_y}\rangle = \delta_{i_x k_x}\delta_{i_y k_y}. \tag{22}$$

The functions $\theta^{\varepsilon}_{j,i_x,i_y}$, $\mu^{\varepsilon}_{j,i_x,i_y}$ are called vaguelettes and have similar properties to wavelets concerning localization and vanishing moments. The latter results from the fact that $\sigma$ is strictly positive at the origin. Since $\sigma(\xi_x,\xi_y) \neq \sigma_x(\xi_x)\,\sigma_y(\xi_y)$, the functions in (20) and (21) are not separable as the two-dimensional scaling function and wavelets.

In the present case it is possible to determine the above functions in Fourier space by means of a symbol, for example,

$$(\widehat{\theta^{\varepsilon}_{j,i_x,i_y}})_{k_x,k_y} = \frac{1}{\sigma(k_x,k_y)}(\widehat{\psi^{\varepsilon}_{j,i_x,i_y}})_{k_x,k_y} \qquad k_x,k_y \in \mathbb{Z} \quad j \geqslant 0 \quad i_x,i_y = 0,\ldots,2^j-1. \tag{23}$$

Since by construction $\langle L\psi^{\varepsilon}_{j,i_x,i_y}, \theta^{\varepsilon}_{j,k_x,k_y}\rangle = \delta_{i_x k_x}\delta_{i_y k_y}$ the functions $\theta^{\varepsilon}_{j,i_x,i_y}$ are used as test functions in a Petrov–Galerkin method for (7). This is equivalent to developing the right-hand side $f$ of this equation into the bi-orthogonal operator-adapted basis as follows:

$$f_{L;J}(x,y) = \langle f, \eta_{0,0,0}\rangle\nu_{0,0,0}(x,y) + \sum_{j=0}^{J-1}\sum_{i_x=0}^{2^j-1}\sum_{i_y=0}^{2^j-1}\sum_{\varepsilon=1}^{3}\langle f, \theta^{\varepsilon}_{j,i_x,i_y}\rangle\mu^{\varepsilon}_{j,i_x,i_y}(x,y). \tag{24}$$

Hence, we define the spaces

$$\boldsymbol{V}_{L;J} = \operatorname{span}\{Lb_{J,i_x,i_y}\}_{i_x,i_y} = \operatorname{span}\{\nu_{J,i_x,i_y}\}_{i_x,i_y}. \tag{25}$$

A cardinal function $S_{L;J,i_x,i_y}$ in $\boldsymbol{V}_{L;J}$ can be defined analogously to (10) by

$$(\widehat{S_{L;J,i_x,i_y}})(k_x,k_y) = \frac{2^{-2J}\sigma(k_x,k_y)\,\widehat{b_{J,i_x,i_y}}(k_x,k_y)}{\sum_{n_x,n_y\in\mathbb{Z}}\sigma(k_x+2^J n_x,k_y+2^J n_y)\,\widehat{b_{J,i_x,i_y}}(k_x+2^J n_x,k_y+2^J n_y)} \tag{26}$$

provided the denominator is different from zero. With these functions a collocation projection onto $\boldsymbol{V}_{L;J}$ can be defined similarly to (15). Observe that $S_L$ can only be decomposed in the same way as $S$ in (16) if $\sigma$ can be factorized accordingly. This is generally not the case. Properties of the vaguelettes and the other operator-adapted basis functions are reported in [22].

Solving (7) by means of the described method is equivalent to calculating a decomposition of $f$ into the bi-orthogonal vaguelette basis and a reconstruction of $u$ in the orthonormal wavelet basis. In other words, one determines

$$d^{\varepsilon}_{j,i_x,i_y} = \langle f_{L;J}, \theta^{\varepsilon}_{j,i_x,i_y}\rangle = \langle Lu_J, \theta^{\varepsilon}_{j,i_x,i_y}\rangle \tag{27}$$

and then uses (17) to compute $u_J$.

In all calculations we used Battle–Lemarié spline wavelets since analytic expressions of the Fourier transforms of the basis functions are available. The cardinal Lagrange function of the spline MRA spaces is well known [35], analytic expressions of the Fourier transforms of the scaling function and wavelets are available [31], and the operator-adapted interpolating functions may be calculated using derivatives of the cotangent function [36]. Furthermore, in the case of a Battle–Lemarié spline MRA all of the above basis functions, even the operator-adapted ones, have exponential decay (cf [36] for a proof). Hence, for a given precision they can be suitably truncated to a finite length. Figure 3 shows iso-lines of wavelets and vaguelettes; (*a*)–(*c*) demonstrate the good localization in physical space of the cardinal Lagrange function (16) and the wavelets (13); (*d*)–(*f*) are concerned with the operator-adapted functions. They illustrate that the operators do not alter the fast decay of the modified basis functions (21) and (26).

### *3.5. Transforms for lacunary bases*

Using the above results we devise the following algorithm to compute the coefficients $d^{\varepsilon}_{j,i_x,i_y}$ according to (27) in the present two-dimensional periodic setting. It is based on the filters

$$D^{j,\varepsilon}_{L;m_x,m_y} = \langle S_{L;j,m_x,m_y}, \theta^{\varepsilon}_{j-1,0,0} \rangle \tag{28}$$

and uses the grids

$$x_{j,i_x,i_y} = \left( \frac{i_x}{2^j}, \frac{i_y}{2^j} \right) \qquad 0 \leqslant i_x, i_y < 2^j \tag{29}$$

which are hierarchically nested for increasing $j$.

*Operator-adapted vaguelette decomposition*

**given** index set $\Lambda_d \subset \Lambda_J =$ for the amplitudes $d^{\varepsilon}_{j,i_x,i_y}$ of a lacunary wavelet basis in $\boldsymbol{V}_J$ with some $J \in \mathbb{N}$.

**0. step** Compute $D^{j,\varepsilon}_L$, $\mu^{\varepsilon}_{j-1,0,0}$, $j = 1, \ldots, J$.
Truncate these in space according to a given precision.

**1. step** Determine the index set $\Lambda_x$ of points $x_{j,i_x,i_y}$ required in the subsequent quadratures.
For $(j, i_x, i_y) \in \Lambda_x$ require the right-hand side at the points $x_{j,i_x,i_y}$ and set

$$f_J(x_{j,i_x,i_y}) = f(x_{j,i_x,i_y}). \tag{30}$$

Set $j = J$.

**2. step** For $(j-1, k_x, k_y, \varepsilon) \in \Lambda_d$

$$d^{\varepsilon}_{j-1,k_x,k_y} = \sum_{(j,i_x,i_y)\in\Lambda_x} f_j(x_{j,i_x,i_y}) D^{j,\varepsilon}_{L;i_x-2k_x,i_y-2k_y}. \tag{31}$$

**3. step** For $(j-1, i_x, i_y) \in \Lambda_x$

$$f_{j-1}(x_{j-1,i_x,i_y}) = f_j(x_{j,2i_x,2i_y}) - \sum_{(j-1,k_x,k_y,\varepsilon)\in\Lambda_d} d_{j-1,k_x,k_y} \mu^{\varepsilon}_{j-1,k_x,k_y}(x_{j-1,i_x,i_y}). \tag{32}$$

**iterate** steps 2 and 3, replacing $j$ with $j-1$ down to $j = 0$.
**final step** compute $c_{0,0,0}$ by the filter $I^{j}_{L;n_x,n_y} = \langle S_{L;j,n_x,n_y}, \eta_{j,0,0} \rangle$ with $j = 0$.

**Remarks.** In the present case $\eta_{0,0,0} = 1/\gamma$ so that $I^0_{L;0,0} = 1/\gamma$. Stopping the decomposition at some $j > 0$ is also possible as discussed in [20]. An adaptive hierarchical wavelet transform is obtained as a special case of the above algorithm setting $L = I$.

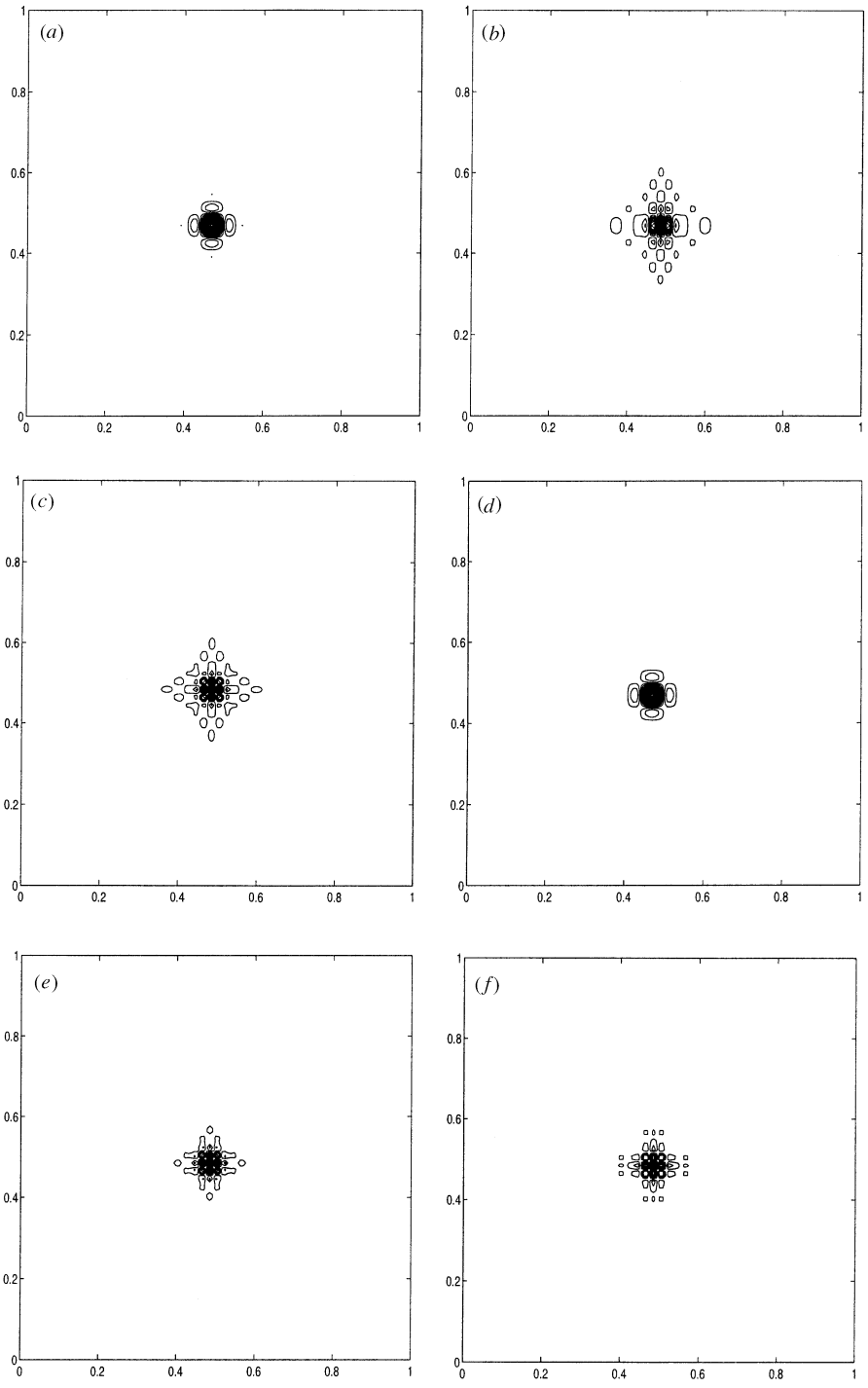


**Figure 3.** Lines of constant value for different functions $f(x, y)$ intervening in the algorithm: (*a*) $S_{j,i_x,i_y}$, (*b*) $\psi^1_{j,i_x,i_y}$, (*c*) $\psi^3_{j,i_x,i_y}$, (*d*) $S_{L;j,i_x,i_y}$, (*e*) $\mu^3_{j,i_x,i_y}$, (*f*) $\theta^3_{j,i_x,i_y}$, with $j = 5, i_x = i_y = 15$ and $\gamma = 150$.

As the nonlinear term $f(u)$ in (27) is evaluated pointwise in physical space with equation (30), the function $u$ given by its wavelet coefficients has to be determined pointwise on a locally refined grid. This requires an inverse wavelet transform for lacunary coefficients to reconstruct $u$ on an adaptive grid $x_{j,i_x,i_y}$ which allows one to apply $f$ to these values.

*Inverse wavelet transform*

**given** coefficients $\{c_{0,0,0}\}_i$, $\{d^{\varepsilon}_{j,k_x,k_y}\}_{(j,k_x,k_y,\varepsilon)\in\Lambda_d}$.
**0. step** Set $j = 0$ and

$$f_0(x_{0,0,0}) = c_{0,0,0}\phi_{0,0,0}(x_{0,0,0}). \tag{33}$$

**1. step** Compute $f_{j+1}$ at even grid points, i.e. for $(j, i_x, i_y) \in \Lambda_x$, $i_x$ and $i_y$ even

$$f_{j+1}(x_{j+1,2i_x,2i_y}) = f_j(x_{j,i_x,i_y}) + \sum_{(j,k_x,k_y,\varepsilon)\in\Lambda_d} d^{\varepsilon}_{j,k_x,k_y}\psi^{\varepsilon}_{j,k_x,k_y}(x_{j,i_x,i_y}). \tag{34}$$

**2. step** Compute $f_{j+1}$ at the remaining odd grid points, i.e. for $(j, i_x, i_y) \in \Lambda_x$, $i_x$ or $i_y$ odd

$$f_{j+1}(x_{j+1,i_x,i_y}) = \sum_{k_x,k_y} f_j(x_{j+1,k_x,k_y})S_{j,k_x,k_y}(x_{j+1,i_x,i_y}) + \sum_{(j,k_x,k_y,\varepsilon)\in\Lambda_d} d^{\varepsilon}_{j,k_x,k_y}\psi^{\varepsilon}_{j,k_x,k_y}(x_{j+1,i_x,i_y}). \tag{35}$$

**iterate** steps 1 and 2 for $j = 1, \ldots, J-1$, where $J-1$ is the finest scale in $\Lambda_d$.

Step 2 is implemented in three parts using the fact that the first sum in (35) contains only one sum on $n_x$ if $i_y$ is even and one sum on $n_y$ if $i_x$ is even due to (16) and (11).

The filters used in the operator-adapted vaguelette decomposition (30) and (31) and the inverse wavelet transform (34) and (35) are closely related to the functions depicted in Figure 3 and hence exhibit exponential decay. Therefore they can be truncated up to some prescribed tolerance. Such a truncation leads for both algorithms to an $O(N)$ operation count, where $N$ denotes the number of active basis functions. Hence the total complexity of the operations in one time step is $O(N)$.

## 4. Numerical results

### *4.1. Computational set-up*

In both, experiments and computations of flame balls, the boundaries have to be sufficiently far from the flame to avoid any disturbance. If this is accomplished, the precise nature of these boundaries is of no importance. Hence, it is possible to choose a periodic approximation in the computations. We consider the domain $(x, y) \in [-X/2, X/2] \times [-X/2, X/2]$ with $X$ sufficiently large. With given equations the solution is then only determined by the initial condition $T(x, y, 0) = T_0(x, y)$, $Y(x, y, 0) = Y_0(x, y)$ which has to be chosen in accordance with the periodic approximation. Here, we introduce an initial flame front by means of the analytic solution for a steady plane flame in the high activation energy limit $\beta \to \infty$ [37]

$$\begin{aligned} T_0(x, y) &= \begin{cases} \exp(r_0 - r) & r \geqslant r_0 \\ 1 & r < r_0 \end{cases} \\ Y_0(x, y) &= \begin{cases} 1 - \exp(Le(r_0 - r)) & r \geqslant r_0 \\ 0 & r < r_0 \end{cases} \end{aligned} \tag{36}$$

where $r = r(x, y)$ is a radial coordinate. In some computations we employed a circular initial condition, whereas in others a local stretching is used to generate an elliptic front. In all computations the derivatives of $T_0$ and $Y_0$ at the boundaries were below machine precision.

Note that the above initialization is well suited for the present two-dimensional case. In three dimensions the asymptotic decay of temperature and concentration is proportional to $1/r$. This is readily obtained from the fundamental solution of a Laplace equation which results from neglecting reaction and radiation in the far field. For the two-dimensional case, however, this approximation is not successful. An approximation of the temperature equation far from the flame of the next higher order by linearizing the radiation term, while neglecting reaction yields a modified Bessel equation. The modified Bessel functions of the second kind solving this equation decay proportional to $\exp(-r)/\sqrt{r}$ which is very close to the employed initial condition. The reasoning for the temperature equation alone suggests the existence of a steady solution with this decay rate at infinity. The concentration equation, however, does not contain a radiation term. It rather raises the question of how the reaction rate is modelled in the limit of ambient temperature, the so-called 'cold boundary difficulty'. If zero reaction is assumed—which is common but contradictory to equation (3)—no truly steady solution exists. On the other hand, the behaviour in the very limit of infinite time and distance is rather of a mathematical nature. The above reasoning certainly holds for large though not necessarily infinite times and distances and is furthermore backed by the results below. For these reasons we use the term quasi-steady to designate the limiting state without technical difficulties.

### *4.2. Circular flame for unitary Lewis number*

As a reference case we start with a computation for $Le = 1$ and $s = 0$ in (1)–(3). Under these conditions plane flames are stable, i.e. they do not exhibit the thermodiffusive instability. This carries over directly to the case of a circular flame if the radius is large. In our computations we also observe this stability for a small radius of the flame starting from an elliptic flame (stretching 1:4). From the initial perturbation the flame soon relaxes to a circle, as shown in figure 4. The ellipticity of the flame decreases from 4 at $t = 0$ to 1.3 at $t = 9$. Further parameters of this computation are $\alpha = 0.8$, $X = 30$, $\Delta t = 10^{-2}$, $J = 7$. Note that the initial deformation can be quite large since, for example, in the case of uniform propagation of the front the ellipticity of the front diminishes for geometrical reasons with increasing diameter.

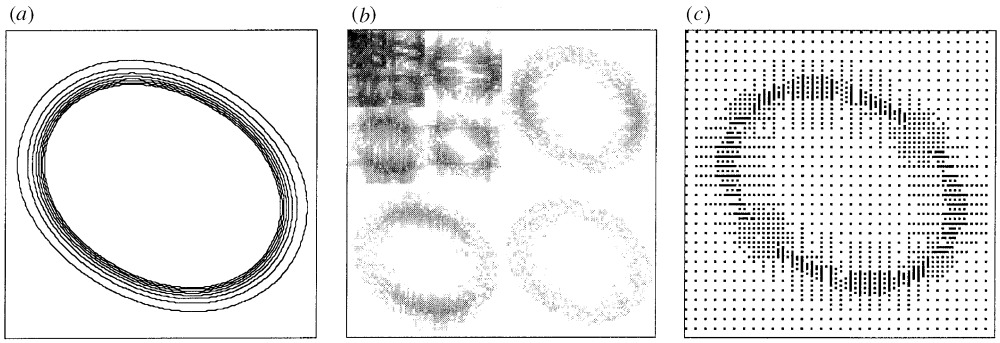


**Figure 4.** Relaxation of an elliptical flame to a circle for $Le = 1$, solution at $t = 9$. (*a*) Lines of constant temperature ($T = 0.1, \ldots, 0.9$). (*b*) Adaptive wavelet basis in the scale-space diagram according to figure 2. A logarithmic scale is used for the absolute value of the retained coefficients. (*c*) Centres of the wavelets used to represent the solution (see text).

Before concentrating in the following sections on the investigation of the physical mechanisms we take this case to illustrate the adaptive wavelet discretization described above. Figure 4(*b*) represents the adaptively selected active wavelets in coefficient space according to the scheme of figure 2. The third part, figure 4(*c*), shows the centres $(x_c, y_c)$ of the active wavelet functions in physical space. Recall that the function $\psi^{\varepsilon}_{j,i_x,i_y}$ is centred around $x_c = (1 - \delta_{\varepsilon,3})/2^{j+1} + i_x/2^j$ and $y_c = (1 - \delta_{\varepsilon,1})/2^{j+1} + i_y/2^j$. At $t = 9$ the index set $\Lambda_d$ comprises 2305 coefficients (out of 16 384 for $J = 7$). The initial ellipse has been inclined by 30° with respect to the coordinate system in order to demonstrate that the wavelet scheme together with the applied adaption strategy does not generate artefacts due to a preferred direction. This is indeed verified by inspection of figure 4.

To validate the adaptive wavelet method for the present combustion problem we compared the solution with a classical Fourier pseudo-spectral method using $128^2$ Fourier modes and the same time discretization as in section 3.1. Both solutions at $t = 9$ are identical up to a difference of 0.1% in the total reaction rate and less than $10^{-4}$ in the temperature. Hence the method is well suited to calculate the evolution of flame balls. We observe that at $t = 9$ only 14% of the basis functions with respect to a regular discretization are needed. Consequently, with dynamic allocation the memory requirement can be substantially reduced. At present, however, the implementation is still crude. It also yields a CPU time larger than necessary with a simulation performed on an IBM AIX RS6000 workstation taking about 1 day. The optimization of the implementation is the subject of current work.

### *4.3. Splitting of flame balls for small Lewis number*

In the following computations the conditions have been chosen to be similar to the experiments in [32] for a 6.5% $H_2$–air flame although an exact reproduction cannot of course be achieved due to the diverse approximations. We set $Le = 0.3$, $\bar{T}_u = 300$ K and $\bar{T}_b = 830$ K, yielding $\alpha = 0.64$ and $\beta = 10$. The extent of the computational domain is $X = 100$ and the maximal resolution of $J = 8$ corresponds to $256^2$ degrees of freedom if the entire wavelet basis is retained. The time step is $\Delta t = 5 \times 10^{-4}$ in all computations.

In [32] the experiments have been conducted with additional $CF_3Br$ in the mixture. This component does not modify the principal reaction but essentially increases the radiation heat loss due to soot production. The experiments in this reference show that with a low concentration of $CF_3Br$, the flame balls exhibit cellular instability. Increased heat loss due to an increased concentration of $CF_3Br$ yields stable flame balls. Similarly to adjusting heat loss by the tracer concentration in the experiments, we use different values of $c$ in (4), here $c = 0, 0.002, 0.01, 0.05, 0.1$. To investigate the instability of the flame balls the initial condition of section 4.2 is applied, accounting for the different Lewis number. Figures 5 and 6 show the results of two such computations with different values of the heat loss parameter $c$. Starting from the initial perturbation an instability develops in figure 5 which results in local quenching of the flame. This is visible from the plots of the reaction rate. The corresponding iso-thermals illustrate the temperature decay in the middle of the flame ball and at the locations of quenching. In figure 6 the instability of the flame leads to a splitting of the initial elliptic flame into two separate smaller flames. After a while these separate again and continue propagating. Since at $t = 30$ the four small flames again have an elliptic shape, one suspects that these might split again. Indeed, this takes place at subsequent times (not shown here).

Together with figure 4 of the previous section, figure 5 illustrates the influence of the Lewis number. The result is in accordance with the theoretical analysis of [4] which predicts (three-dimensional) instability for small Lewis number and low heat loss. For $c < 10^{-2}$ the solution is qualitatively similar to that reported in figure 5. Even with vanishing heat loss

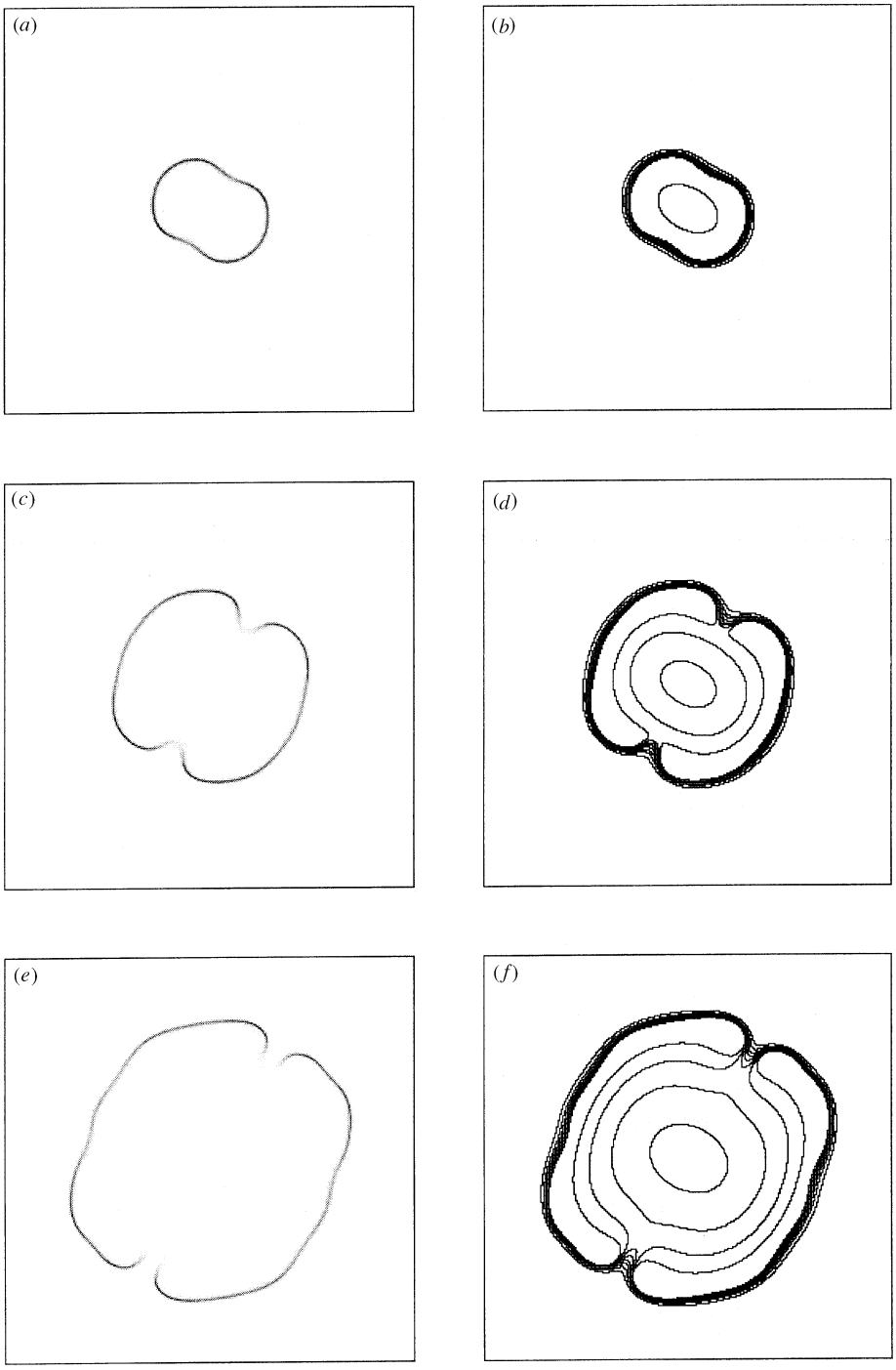


**Figure 5.** Flame ball with $Le = 0.3$, $c = 0.01$: (*a*), (*c*) and (*e*) reaction rate at times $t = 10, 20, 30$, (*b*), (*d*) and (*f*) corresponding iso-thermals $T = 0.1, 0.2, \ldots, 1$.

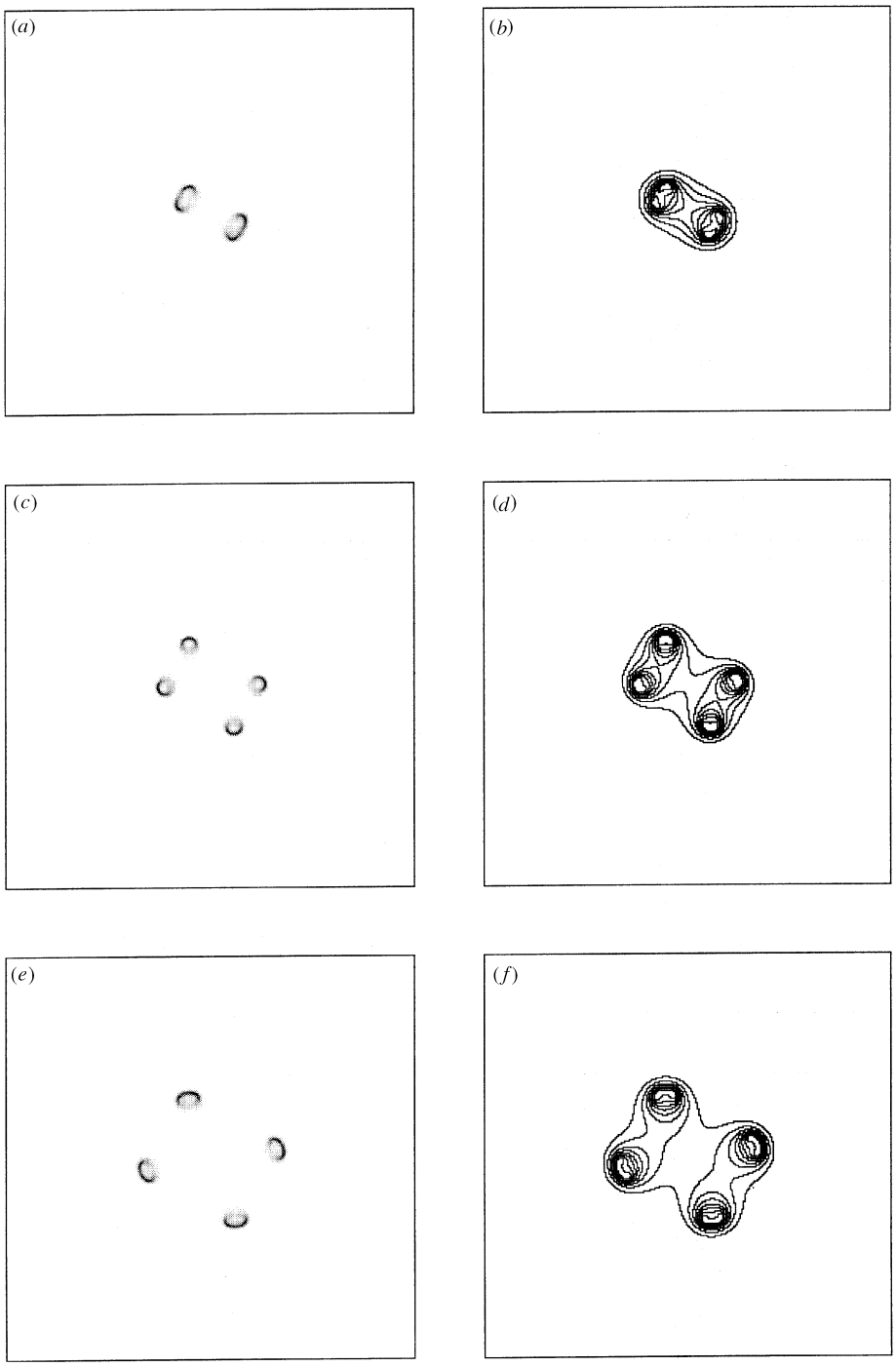


**Figure 6.** Flame ball with $Le = 0.3$, $c = 0.05$: (*a*), (*c*) and (*e*) reaction rate at times $t = 10, 20, 30$, (*b*), (*d*) and (*f*) corresponding iso-thermals $T = 0.1, 0.2, \ldots, 1$.

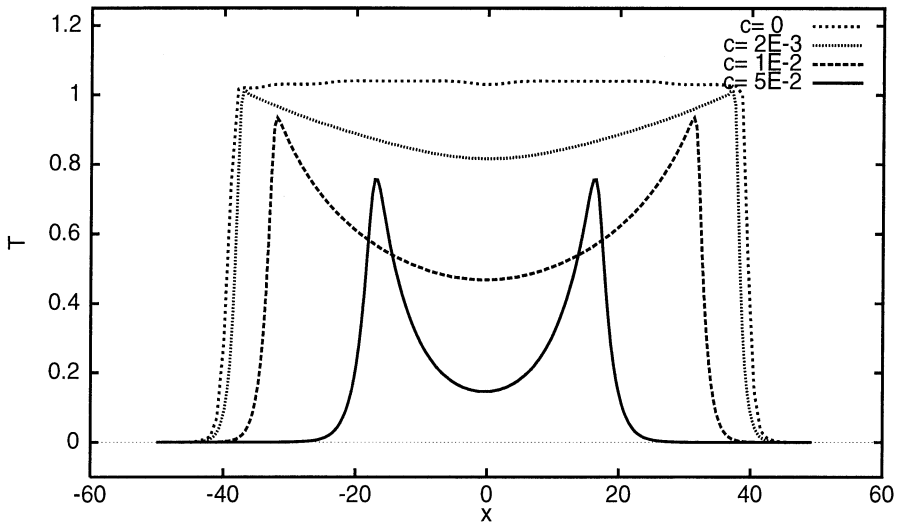


**Figure 7.** Horizontal cuts at $y = 0$ through the temperature field at $t = 30$ for different amounts of heat loss: $c = 0, 0.002, 0.01, 0.05$ (top to bottom at $x = 0$).

**Table 1.** Influence of heat loss on diameter, maximal temperature and maximal reaction rate at $t = 30$ (see text).

| Heat loss $c$ | $T_{\max}$ | $\omega_{\max}$ | $W_x\|_{T=0.8}$ | $\overline{v_f}$ |
|---|---|---|---|---|
| 0 | 1.11 | 5.65 | 80.4 | 2.42 |
| 0.002 | 1.10 | 5.34 | 78.5 | 2.36 |
| 0.01 | 1.06 | 4.27 | 68.9 | 2.04 |
| 0.05 | 0.89 | 1.51 | 35.6 | 0.93 |

similar undulations and local quenching of the reaction front are observed. This behaviour has also been obtained by Denet and Haldenwang [14] in their computations of an adiabatic flame in a planar channel with $Le = 0.2$, $\alpha = 0.8$, $\beta = 10$.

The influence of radiation can be assessed by comparing figures 5 and 6. The only difference in these two computations is an increase of $c$ by a factor of 5, from 0.01 to 0.05. For $c = 0.1$ the flame is extinguished. Figure 7 displays a horizontal cut in the middle of the domain through the temperature fields of figures 5 and 6 at $t = 30$, and two further cases not represented in other figures. The influence of the radiation heat loss is nicely visible: in the interior of the flame ball the temperature is reduced, heat flows from the flame front inwards to balance the loss. Second, the distance which the flames have travelled is reduced leading to different locations of the front at $t = 30$. In that respect it is also instructive to superpose the plots of figures 5 and 6 at corresponding times. The reaction zones of the latter lie exactly in the centres of the undulations in figure 5. More quantitative information is given in table 1 where the maxima of temperature and reaction rate over the whole domain are displayed. Observe that for low radiation, locally the temperature exceeds the adiabatic flame temperature. This is due to the high diffusivity of species related to the present Lewis number. Hence, additional species are transported to the flame where they induce additional heating which is not compensated by diffusive heat loss. The values of $T_{\max} > 1$ reported in the table typically occur in the tips of the flames near the zones of local extinction. A similar behaviour can also be observed in

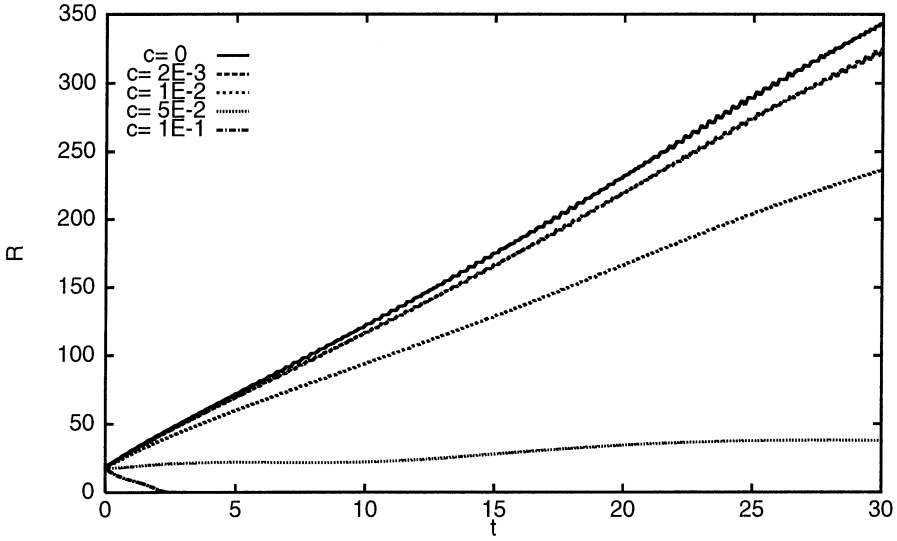


**Figure 8.** Integral of the reaction rate $R$ versus time for different amounts of heat loss: $c = 0, 0.002, 0.01, 0.05, 0.1$ (top to bottom).

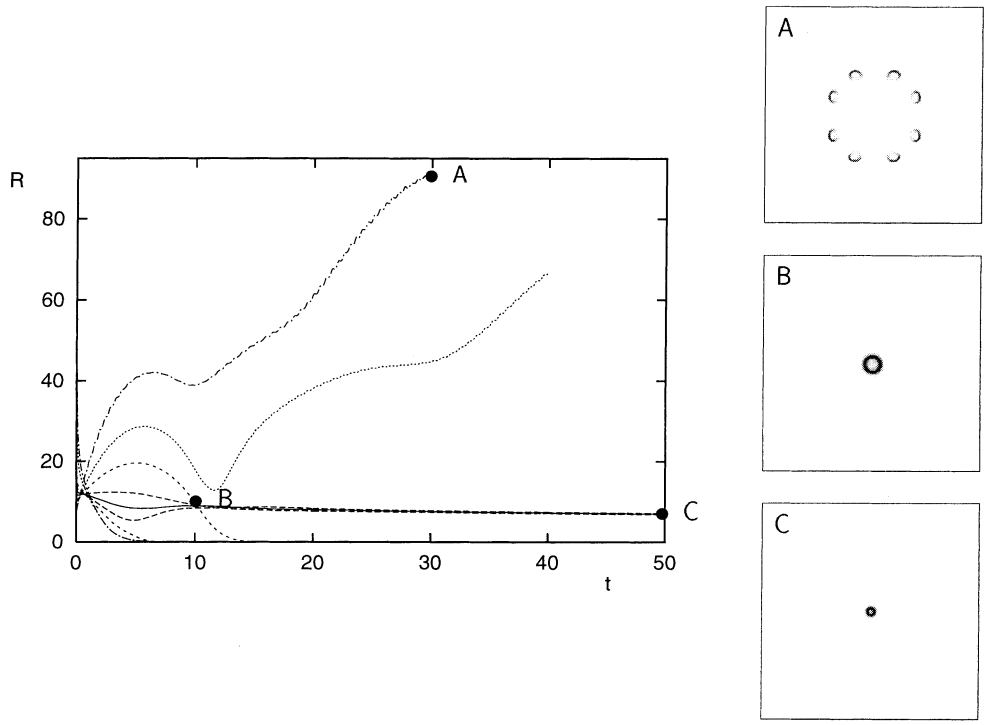


**Figure 9.** Different scenarios for the evolution of the computed flame balls with $c = 0.05$. Left, evolution of the total reaction rate with different initial radii. At $t = 5$ the curves can be labelled from above with $r_0 = 1, 1.25, 1.5, 1.8, 2, 2.5, 4, 5$, respectively. Right, fields of the reaction rate at typical points indicated in the evolution diagram.

the temperature plots of [14]. The quantity $W_x|_{T=0.8}$ is the maximal extent in the $x$-direction of the $T = 0.8$ temperature level line at $t = 30$. Comparison to its initial value 7.7 yields an average propagation rate of the flame $\overline{v_f}$ reported in the last column of the table.

The overall reaction rate $R(t) = \int \omega(x, y, t)\,\mathrm{d}x\,\mathrm{d}y$ in figure 8 gives a complementary report on the dynamics. In a first phase, up to around $t = 1$, the inner structure of the flame adjusts to the finite value of $\beta$. Subsequently, the flame propagates outward, more or less rapidly according to the strength of the radiation. Due to the undulations of the flame front the increase of the total reaction rate is not linear as it would be in the case of a steadily expanding circular flame. Finally, we note that in a parallel work Kagan and Sivashinsky [26] have examined the influence of radiation on a straight flame described by the same combustion model. Their observations agree very well with the present results.

### *4.4. Quasi-steady flame balls*

After studying the influence of the amount of radiation in the previous section we now fix the prefactor to $c = 0.05$ and report on the computation of quasi-steady flame balls. Hence, a circular initial condition was employed and a large number of computations with different initial radii have been performed. These are summarized in figure 9, showing the evolution of the total reaction rate $R(t)$ as well as selected typical fields.

During the initial phase of the computations the inner structure of the flame adjusts to the employed parameters so that its physical significance is low. After a very short time, however, a physically meaningful solution is computed. The figure then reveals an interesting bifurcation. For certain initial conditions with $r_0$ around 2, indeed a quasi-steady flame ball develops. In a transient phase a temporarily smaller or larger circular flame forms, but the quasi-steady state

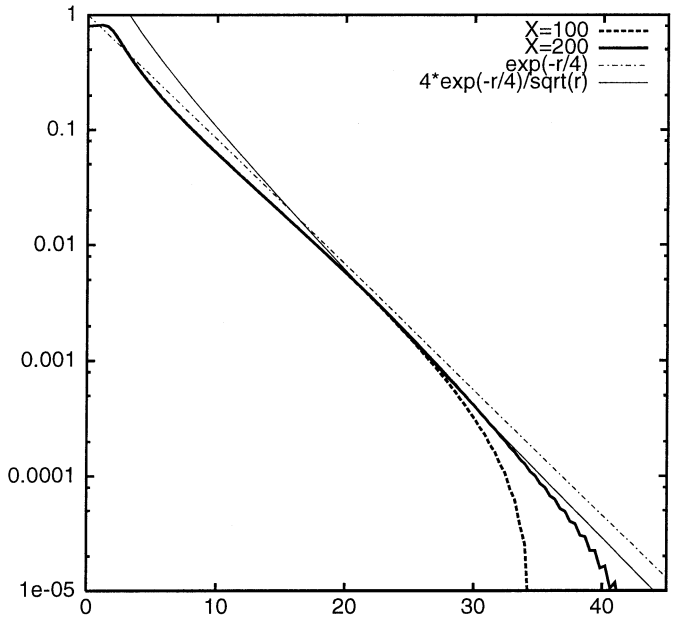


**Figure 10.** Cuts through the temperature field for $y = 0$, $t = 50$, $c = 0.05$ computed with normal domain size $X = 100$ and doubled size. The decay is compared to $T_1(r) = \exp(-r)$ and $T_2(r) = 4\exp(-r)/\sqrt{r}$.

is the same for all initial conditions within a certain range of attraction (figure 9C). This flame has a diameter of about 3 in dimensionless units and persists for a long time (left-hand picture of figure 9). In this stage the total reaction rate is very slowly decreasing so that the flame ball is not absolutely steady. The limit of infinite time cannot be computed due to periodicity and the discussion in section 4.1. For verification we have also repeated the computation with $r_0 = 2$, doubling the domain size in each direction and obtained the same steady solution. Figure 10 displays cuts through the temperature field of these computations. It also contains two curves proportional to $\exp(-r)$ and $\exp(-r)/\sqrt{r}$, respectively, which justify the choice of the initial condition and the arguments in section 4.1.

Figure 9 shows that a certain perturbation of the flame can be attenuated, driving it back to the stable state. If, however, this perturbation is too strong the solution becomes unstable. This can take place in several ways. If the flame is too large by initialization it extinguishes merely without changing its radius as encountered for $r_0 = 4$ and 5. A similar behaviour

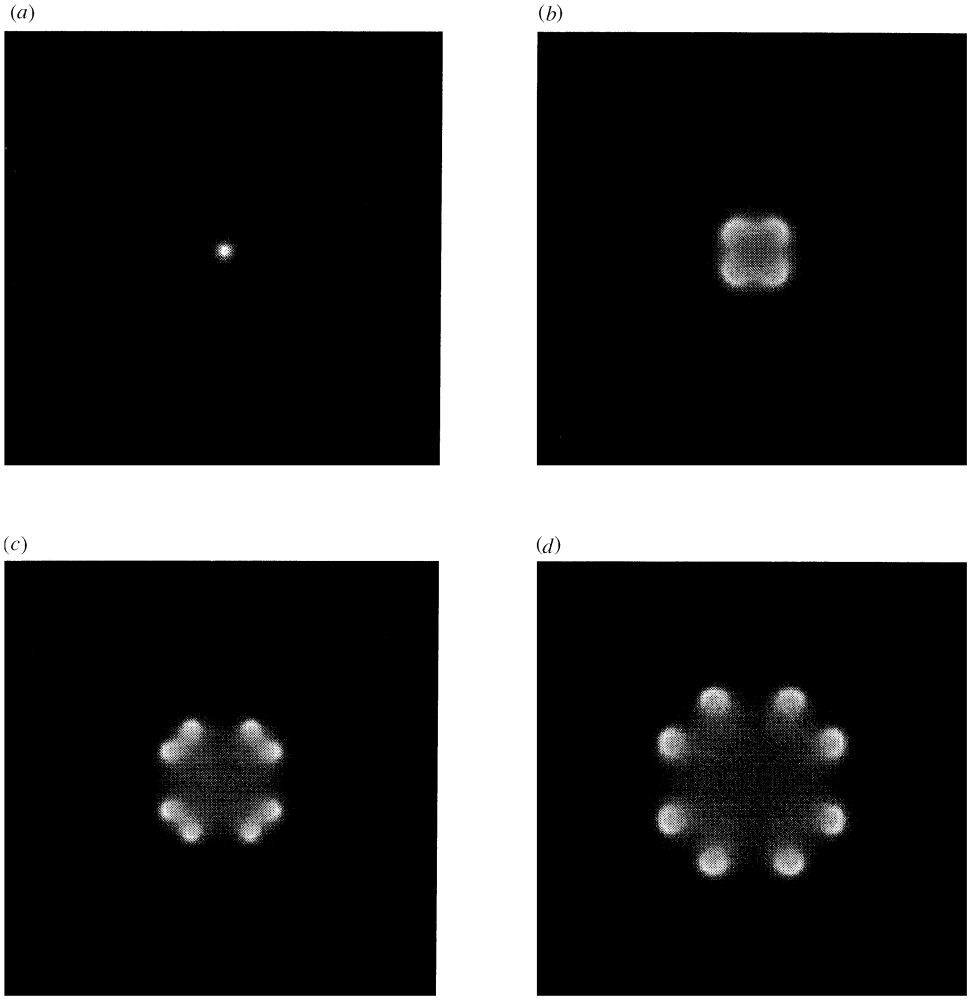


**Figure 11.** Flame balls with $Le = 0.3$, $c = 0.05$ and circular initial condition with $r_0 = 1$. Pictures (*a*), (*b*), (*c*) and (*d*) show the temperature field at times $t = 0$, 10, 20, 30, respectively.

is observed if the flame increases too much during the transient phase, while still remaining circular as with $r_0 = 1.5$ (figure 9B). A third type of evolution is related to a splitting of the flame in smaller and smaller cells (figure 9A). The observed dissociation is extremely similar to the one of figure 6 obtained with an elliptic initial front and is depicted in figure 11. It shows that, unlike in the previous section, the flame directly splits up into four cells. Their orientation is determined by the tiniest details or noise in the computation and is no indication of a biased method. This is proven by the results of the previous section. In later stages of the computation the eight cells continue propagating slowly outward. At $t = 50$ they again exhibit a half-elliptic shape which is an indication of the advent of further splitting. Nevertheless, the computation was stopped due to increasing, though still only slight, influence of the periodic boundary conditions.

This computation suggests that the splitting of flame balls in the considered parameter regime may continue *ad infinitum*. On the other hand, it might be proposed that the observed dissociation is just a transition to an ensemble of circular quasi-steady flame balls all having the stable radius obtained above. At present we cannot decide on the asymptotic state for large times. In any case the existence of an inner region within the ring of cells containing partially burnt gas and an outer region with unburnt gas introduces a considerable asymmetry which rules out the second possibility. Whether for some values of the parameters a quasi-steady solution in the form of a ring of (non-circular) cells exists remains an open question.

The presented results demonstrate that quasi-steady flame balls can be obtained in two dimensions. This is qualitatively the same as in the spherical case. As far as we know a complete stability analysis for the two-dimensional configuration has not been reported up to now. It can certainly be accomplished with similar techniques, as employed in [3–5], but is beyond the scope of the present paper.

## 5. Conclusion

The present paper describes a two-dimensional adaptive wavelet algorithm for elliptic PDEs. It makes use of local hierarchical wavelet collocation and employs a truly two-dimensional operator-orthogonal multiresolution analysis. We show that the developed adaptive method is a useful method for the computation of two-dimensional flames. The employed basis functions are selected dynamically, which induces local refinement only in the propagating reaction zone. Hence, the number of degrees of freedom can be reduced significantly without losing numerical accuracy. Although the method is fully developed its coding is still experimental. It inhibits a realistic assessment of the method's cost (theoretically $O(N)$) as the computing time, in particular with adaptive methods, depends highly on aspects of the implementation. This is the subject of our current work.

The paper reports on various computations of thermodiffusive flames. In particular, we have studied the influence of the Lewis number, the strength of radiative losses and the initial form and radius on such flames. Part of the simulations were concerned with splitting flame balls. Although the physical mechanisms involved are somewhat different, as discussed in the text, the calculated patterns, such as shown in figure 11, are strikingly similar to photographs taken in experiments (see, e.g., figure 1 in [32]). Furthermore, we have succeeded in obtaining quasi-steady flame balls. Computations with different initial radii give additional information on the range of attraction of such flames.

Using direct simulations it is possible to investigate the full nonlinear behaviour of flame balls even in the case of large deformations and splitting. This will be further exploited. Future computations could also employ different models for radiation. In [28] a PDE for the heat loss, the linearized Eddington equation, is the basis for an asymptotic analysis. Since it has a

similar form to the equations presently solved for temperature and species in each time step the proposed wavelet method can be extended to solve such an equation together with (1)–(3). This gives the possibility to compare the influence of different radiation models. By direct simulation it can be done for both large and small activation energy. The computation of flame balls in three dimensions is the subject of current research. Preliminary results show a similar pattern formation and will be presented in a forthcoming paper.

## Acknowledgments

The authors thank P Haldenwang and P Ronney for stimulating discussions during the course of this work. Partial support by the Commission of the European Communities Contract No FMRX-CT 98-0184 TMR Project 'Wavelets in Numerical Simulation' is acknowledged.

## References

[1] Bertoluzza S and Naldi G 1994 Some remarks on wavelet interpolation *Comput. Appl. Math* **13** 13–32
[2] Buckmaster J 1993 The structure and stability of laminar flames *Annual Reviews in Fluid Mechanics* vol 25 pp 21–53 (Palo Alto, CA: Annual Reviews)
[3] Buckmaster J, Gessman R and Ronney P 1992 The three-dimensional dynamics of flame-balls *24th Int. Symp. on Combustion* pp 53–9 (Pittsburgh, PA: Combustion Institute)
[4] Buckmaster J, Joulin G and Ronney P 1990 The structure and stability of nonadiabatic flame-balls *Combust. Flame* **79** 381–92
[5] Buckmaster J, Joulin G and Ronney P 1991 The structure and stability of nonadiabatic flame-balls: II effects of far-field losses *Combust. Flame* **84** 411–22
[6] Buckmaster J, Smooke M and Giovangili V 1993 Analytical and numerical modelling of flame-balls in hydrogen–air mixtures *Combust. Flame* **94** 113–24
[7] Buckmaster J and Weeratunga S 1984 The stability and structure of flame-bubbles *Combust. Sci. Technol.* **35** 287–96
[8] Bush W B and Fendel F E 1970 Asymptotic analysis of laminar flame propagation for general Lewis number *Combust. Sci. Technol.* **1** 421–28
[9] Cai W and Wang J 1996 Adaptive multiresolution collocation methods for initial boundary value problems of nonlinear PDEs *SIAM J. Numer. Anal.* **33** 937–70
[10] Chui C K 1992 *An Introduction to Wavelets* (New York: Academic)
[11] Dahlke S and Weinreich I 1993 Wavelet–Galerkin methods, an adapted biorthogonal wavelet basis *Constr. Approx.* **9** 237–62
[12] Dahmen W 1997 Wavelet and multiscale methods for operator equations *Acta Numerica* **6** 55
[13] Daubechies I 1992 *Ten Lectures on Wavelets* (Philadelphia, PA: SIAM)
[14] Denet B and Haldenwang P 1989 A local extinction of the thermodiffusive premixed flame at low Lewis number ed A Dervieux and B Larrouturou *Numerical Combustion* (*Lecture Notes in Physics* vol 351) (Berlin: Springer) pp 223–32
[15] Dervieux A, Larrouturou B and Peyret R 1989 On some adaptive numerical approaches of thin-flame propagation problems *Comp. Fluids* **17** 39–60
[16] Deshaies B and Joulin G 1984 On the initiation of a spherical flame kernel *Combust. Sci. Technol.* **37** 99–116
[17] DeVore R A, Jawerth B and Popov V 1992 Compression of wavelet decomposition *Am. J. Math.* **114** 737–85
[18] Donoho D L 1993 Unconditional bases are optimal bases for data compression and statistical estimation *Appl. Comput. Harmonic Anal.* **1** 100–15
[19] Farge M, Kevlahan N, Perrier V and Schneider K 1998 Turbulence analysis, modelling and computing using wavelets *Wavelets and Physics* (Cambridge: Cambridge University Press)
[20] Fröhlich J and Schneider K 1994 An adaptive wavelet Galerkin algorithm for one- and two-dimensional flame computations *Eur. J. Mech.* B **13** 439–71
[21] Fröhlich J and Schneider K 1996 Numerical simulation of turbulent flows in an adaptive wavelet basis *Appl. Comput. Harmonic Anal.* **3** 393–7
[22] Fröhlich J and Schneider K 1997 An adaptive wavelet–vaguelette algorithm for the solution of nonlinear PDEs *J. Comput. Phys.* **130** 174–90
[23] Jawerth B and Sweldens W 1994 An overview of wavelet based multiresolution analyses *SIAM Rev.* **36** 377–412

[24] Joly P, Maday Y and Perrier V 1994 Towards a method for solving partial differential equations by using wavelet packets *Comput. Methods Appl. Mech. Engng* **116** 301–7
[25] Kagan L and Sivashinski G 1996 Incomplete combustion in nonadiabatic premixed gas flames *Phys. Rev.* E **53** 6021–7
[26] Kagan L and Sivashinski G 1997 Self-fragmentation of nonadiabatic cellular flames *Combust. Flame* **108** 220–6
[27] Liandrat J and Tchamitchian Ph 1990 Resolution of the 1-D regularized Burgers equation using a spatial wavelet approximation algorithm and numerical results *Technical report ICASE*
[28] Lozinski D, Buckmaster J and Ronney P 1994 Absolute flamability limits and flame-balls *Combust. Flame* **97** 301–16
[29] Maday Y, Perrier V and Ravel J Ch 1991 Adaptivité dynamique sur bases d'ondelettes pour l'approximation d'équations aux derivées partielles *C. R. Acad. Sci., Paris I* **312** 405–10
[30] Meyer Y 1990 *Ondelettes et Opérateurs I/II* (Paris: Hermann)
[31] Perrier V and Basdevant C 1989 La décomposition en ondelettes périodiques, un outil pour l'analyse de champs inhomogènes. Théorie et algorithmes *Rech. Aérosp.* **3** 53–67
[32] Ronney P 1990 Near-limit flame structures at low Lewis number *Combust. Flame* **82** 1–14
[33] Ronney P March 1998 Premixed laminar and turbulent flames at microgravity *Space Forum* submitted
[34] Ronney P D and Sivashinsky G I 1989 A theoretical study of propagation and extinction of nonsteady spherical flame fronts *SIAM J. Appl. Math.* **49** 1029–46
[35] Schoenberg I J 1969 Cardinal interpolation and spline functions *J. Approx. Theory* **2** 167–206
[36] Tchamitchian Ph, Schneider K and Fröhlich J in preparation
[37] Williams F A 1985 *Combustion Theory* (Menlo Park, CA: Benjamin-Cummings)
[38] Williams J R and Amaratunga K 1995 A multiscale wavelet solver with O($n$) complexity *J. Comput. Phys.* **122** 30–8
[39] Wu M and Ronney P 1998 Numerical simulation of diluent effects on flame balls *Technical report* Department of Mechanical Engineering, University of Southern California, CA
[40] Zeldovich Ya B 1944 *Theory of Combustion and Detonation of Gases* (Academy of Sciences)